

CERN-PH-EP-2016-040

24 November 2016

Systematic studies of correlations between different order flow harmonics in Pb–Pb collisions at $\sqrt{s_{\text{NN}}} = 2.76$ TeV

ALICE Collaboration *

Abstract

The correlations between event-by-event fluctuations of amplitudes of anisotropic flow harmonics in Pb–Pb collisions at $\sqrt{s_{\text{NN}}} = 2.76$ TeV ~~were~~ have been measured with the ALICE detector at the Large Hadron Collider. The results were obtained with the new multi-particle cumulant method ~~–The dubbed symmetric cumulants.~~ This method is robust against systematic biases originating from non-flow effects. The centrality dependence of correlation between the higher ~~Fourier-order~~ harmonics (v_3 , v_4 , v_5) and the lower order harmonics (v_2 , v_3) as well as the transverse momentum dependence of v_3 – v_2 and v_4 – v_2 correlations are presented. The results are compared to ~~predictions~~ calculations from viscous hydrodynamics and A Multi-Phase Transport ~~model~~ (AMPT) models. The comparisons to viscous hydrodynamic models demonstrate that the different order Fourier harmonic correlations respond differently to the initial conditions or the shear viscosity to the entropy density ratio (η/s and the). ~~The~~ The small η/s regardless of initial conditions is ~~flavored~~ flavored and the small η/s with the AMPT initial condition is closest to the results. v_3 – v_2 and v_4 – v_2 correlations show moderate p_T dependence in mid central collisions. This might be an indication of possible viscous corrections for the equilibrium distribution at hadronic freeze-out which is the least understood part of hydrodynamic calculations.

Together with the existing measurements of individual flow harmonics the presented results provide further constraints on initial conditions and the transport properties of the system produced in heavy-ion collisions.

1 Introduction

The main emphasis of the ultra-relativistic ~~heavy-ion-heavy-ion~~ collisions at the Relativistic Heavy Ion Collider (RHIC) and the Large Hadron Collider (LHC) is to study deconfined phase of the strongly interacting ~~nuclear~~ matter, the Quark-Gluon Plasma (QGP). This matter exhibits strong collective and anisotropic flow in the ~~transverse-plane-plane~~ transverse to the beam direction, which is driven by the ~~anisotropic~~ pressure gradients, ~~with-resulting in~~ more particles emitted in the direction of the largest gradients. The large elliptic flow discovered at RHIC energies [?] continues to increase also ~~in-at~~ LHC energies [? ?]. This has been predicted by calculations utilising viscous hydrodynamics [? ? ? ? ?].

These calculations also demonstrated that the shear viscosity to the entropy density ratio (η/s) of ~~strongly interacting-matter-QGP~~ is close to a universal lower bound $1/4\pi$ [?] in ~~heavy-ion-heavy-ion~~ collisions at RHIC and LHC energies.

The temperature dependence of the η/s has some generic features that most of the known fluids obey. ~~One-For instance, one~~ such general behavior is that the ratio typically reaches its minimum value close to the phase transition region [?]. It was shown, using kinetic theory and quantum mechanical considerations [?], that $\eta/s \sim 0.1$ would be ~~an-the correct~~ order of magnitude for the lowest possible shear viscosity to entropy ratio ~~value found~~ in nature. Later it was ~~found-that-one-can-calculate-demonstrated that~~ an exact lower bound $(\eta/s)_{\min} = 1/4\pi \approx 0.08$ ~~can be caculated~~ using the AdS/CFT correspondence [?]. Hydrodynamical simulations ~~supports-support~~ as well the view that the QGP matter ~~indeed~~ is close to that limit [?]. This in turn may have ~~an-important-implications-to-important implications for~~ other fundamental physics goals. It is argued that such a low value might imply that thermodynamic trajectories for the expanding matter would lie close to the ~~QCD-quantum chromodynamics (QCD)~~ critical end point, which is another subject of intensive experimental quest [?].

Anisotropic flow [?] is traditionally quantified with harmonics v_n and corresponding symmetry plane angles ψ_n in the Fourier series decomposition of particle azimuthal distribution in the plane transverse to the beam direction [?]:

$$E \frac{d^3N}{dp^3} = \frac{1}{2\pi} \frac{d^2N}{p_T dp_T d\eta} \left\{ 1 + 2 \sum_{n=1}^{\infty} v_n(p_T, \eta) \cos[n(\varphi - \Psi_n)] \right\}, \quad (1)$$

where E , N , p , p_T , φ and η are the energy, particle yield, total momentum, transverse momentum, azimuthal angle and pseudorapidity of particles, respectively, and Ψ_n is the azimuthal angle of the symmetry plane of the n^{th} -order harmonic. The n^{th} -order flow coefficients are denoted as v_n and can be ~~derived-calculated~~ as $v_n = \langle \cos[n(\varphi - \Psi_n)] \rangle$, where the brackets denote an average over all particles in all events.

The anisotropic flow in heavy-ion collisions is understood as hydrodynamic response ~~to-spatial-deformation of produced matter to spatial deformations~~ of the initial ~~density-profile~~ energy density profile [?]. This profile fluctuates event-by-event due to fluctuations of the positions of the constituents inside the colliding nuclei, which in turn implies that the flow also fluctuates [? ?]. The recognition of the importance of flow ~~fluctuation-fluctuations~~ has led to triangular flow and higher flow harmonics [? ?] as well as the correlations between different Fourier harmonics ~~[?]-[? ?]~~ [? ?].

The higher order harmonics are expected to be particularly sensitive to fluctuations in the initial conditions and to the η/s [? ?], while correlations have the potential to discriminate the two respective contributions to anisotropic flow development [?]. And the v_n distributions carry detailed information about the initial energy density profile [? ?].

However, difficulties on extracting ~~the-shear-viscosity-in-heavy-ion-has-been-realized-since- η/s in heavy-ion collisions can be attributed mostly to the fact that~~ it strongly depends on the specific choice of

the initial conditions [? ? ?]. The viscous effects reduce the magnitude of the elliptic flow. Furthermore, the magnitude of η/s used in these calculations should be considered as an average over the temperature history of the expanding fireball as it is known that η/s of other fluids depends on temperature. In addition, part of the elliptic flow can also originate from the hadronic phase [? ? ?]. Therefore, knowledge of both the temperature dependence and the relative contributions from the partonic and hadronic phases should be understood better to quantify η/s of the partonic fluid.

~~The higher harmonics~~ (An important input to the hydrodynamic simulations is the distribution of energy density in the transverse plane (the initial density profile), which is usually estimated from the probability distribution of nucleons in the incoming nuclei. This initial energy density profile can be quantified by calculating the distribution of the spatial eccentricity [? ? ?].

$$\varepsilon_n e^{in\Phi_n} = -\{r^n e^{in\phi}\} / \{r^n\} \quad (2)$$

where the curly brackets denote the average over the transverse plane, i.e., $\{\dots\} = \int dx dy e(x, y, \tau_0) (\dots)$, r is the distance to the system's center of mass, $e(x, y, \tau_0)$ is the energy density at the initial time τ_0 , and Φ_n is the participant plane angle (see Ref. [? ? ?]). There are experimental and theoretical evidences [? ? ?] that the harmonic coefficients, v_2 and v_3 , are to a good approximation linearly proportional to the deformations in the initial energy density in the transverse plane (e.g. $v_n \propto \varepsilon_n$ for $n=2$ or 3). v_4 and higher order flow coefficients can arise from initial anisotropies in the same harmonic [? ? ? ?] (linear response) or can be induced by lower-order harmonics [? ? ?] (nonlinear response). Therefore the higher harmonics ($n > 3$) ~~are~~ could be understood as superpositions of linear and nonlinear responses, through which they are correlated with ~~lower-order harmonics~~ [? ? ?] lower order harmonics [? ? ? ?]. When the ~~harmonic order~~ order of harmonic is large, the nonlinear response contribution in viscous hydrodynamics is dominant and become larger for more peripheral collisions [? ? ?]. The magnitude of the viscous corrections as a function of p_T for v_4 and v_5 is sensitive to ansatz used for the viscous distribution function, δf , a correction for the equilibrium distribution at hadronic freeze-out [? ?]. Hence the studies of the higher order ($n > 3$) to lower order (v_2 or v_3) harmonic correlations and their p_T dependence can help to understand the viscous correction to the momentum distribution at hadronic freeze-out which is probably the least understood part of hydrodynamic calculations [? ? ?].

Recently ~~we~~, ALICE Collaboration measured for the first time the new multiparticle observables, the Symmetric 2-harmonic 4-particle Cumulants (SC), which quantify the relationship between event-by-event fluctuations of two different flow harmonics [? ? ?]. The new observables are particularly robust against few-particle non-flow correlations and they provide orthogonal information to recently analysed symmetry plane correlators [? ? ?]. It was demonstrated that they are sensitive to the η/s of the ~~expanding medium and~~ expanding medium and therefore simultaneous descriptions of different order harmonic correlations would constrain both the initial conditions and the medium properties. In this article, we have extended the ~~that~~ analysis to higher order Fourier harmonic (up to ~~5th~~ 5th order) correlations as well as to p_T dependence of correlations for the lower order ~~harmonic~~ harmonics (v_3-v_2 and v_4-v_2). We also include ~~a systematic comparison~~ extensive comparisons to hydrodynamic and AMPT ~~models~~ model calculations. In Sec. ?? we present the details of the analysis methods. The experimental setting and measurements are described in Sec. ?? and the sources of systematic uncertainties are explained in Sec. ??. ~~Various theoretical models used in the article are described in Sec. ??.~~ The results of the measurements are presented in Sec. ??. In Sec. ?? we present comparisons to theoretical calculations. Sec. ?? summarizes our findings.

2 Data Analysis

2.1 Experimental Observables

While from existing measurements an estimate can be placed on the average value of QGP's η/s , both at RHIC and LHC energies, what remains completely unknown is how the η/s of QGP depends on temperature (T). This study has been just initiated by the theorists in Ref. [?], where the first (and only rather qualitative) possibilities were investigated (see Fig. 1 therein). The emerging consensus of late is that it is unlikely that the study of individual flow harmonics v_n will reveal the details of $\eta/s(T)$ dependence. In fact, it was demonstrated already in the initial study [?] that different $\eta/s(T)$ parameterizations can lead to the same centrality dependence of individual flow harmonics. In Ref. [?] new flow observables were introduced by the theorists, which quantify the degree of correlation between two different harmonics v_m and v_n . The initial success of these new observables was attributed to their potential to discriminate for the first time the two respective contributions to anisotropic flow development—from initial conditions and from the transport properties of the QGP [?]. Therefore their measurement in turn would enable the experimental verification of theoretical predictions for individual stages of heavy-ion evolution independently. Besides this advantage, it turned out that correlations of different flow harmonics are sensitive to the details of $\eta/s(T)$ dependence [?], to which individual flow harmonics are nearly insensitive [?].

For technical reasons, discussed in detail in Refs. [? ?], the correlations between different flow harmonics cannot be studied experimentally with the same set of observables introduced by the theorists in Ref. [?]. The technical details are elaborated in Ref. [?], while the first measurements of SC observables were recently released by ALICE Collaboration in Ref. [?].

The SC observables are defined as:

$$\begin{aligned} \langle \langle \cos(m\phi_1 + n\phi_2 - m\phi_3 - n\phi_4) \rangle \rangle_c &\equiv \langle \langle \cos(m\phi_1 + n\phi_2 - m\phi_3 - n\phi_4) \rangle \rangle \\ &\quad - \langle \langle \cos[m(\phi_1 - \phi_2)] \rangle \rangle \langle \langle \cos[n(\phi_1 - \phi_2)] \rangle \rangle \\ &\approx \end{aligned} \quad (3)$$

with the condition $m \neq n$ for two positive integers m and n . The complete discussion can be found in Section IV C of Ref. [?].

$SC(m, n)$ can be normalized with the product $\langle v_m^2 \rangle \langle v_n^2 \rangle$ to obtain *normalized symmetric cumulants* [? ?], which we denote by $NSC(m, n)$, i.e.

$$NSC(m, n) \equiv \frac{SC(m, n)}{\langle v_m^2 \rangle \langle v_n^2 \rangle}. \quad (4)$$

Normalized symmetric cumulants reflect only the degree of the correlation which is expected to be insensitive to the magnitudes of v_m and v_n , while $SC(m, n)$ contains both the degree of the correlation and individual v_n harmonics. In Eq. (??) the products in the denominator are obtained with two-particle correlations and using a pseudorapidity gap of $|\Delta\eta| > 1.0$ to suppress biases from few-particle nonflow correlations. On the other hand, in the two two-particle correlations which appear in the definition of $SC(m, n)$ in Eq. ?? the pseudorapidity gap is not needed, since nonflow is suppressed by construction in SC observable, as the study based on HIJING model has clearly demonstrated in Ref. [?].

The first measurements of SC observables have revealed that fluctuations of v_2 and v_3 are anti-correlated, while fluctuations of v_2 and v_4 are correlated in all centralities [?]. However, the details of the centrality

dependence differ in the fluctuation-dominated (most central) and the geometry-dominated (mid-central) regimes [?]. Most importantly, the centrality dependence of SC(4,2) cannot be captured with the constant η/s dependence, indicating clearly that the temperature plays an important role in describing QGP's η/s dependence in various stages of heavy-ion evolution. These results were also used to discriminate between different parameterizations of initial conditions and it was demonstrated that in the fluctuation-dominated regime (in central collisions) MC-Glauber initial conditions with binary collisions weights are favored over wounded nucleon weights [?].

The SC observables provide orthogonal information to recently measured symmetry plane correlators in Refs. [? ? ?]. This statement does not exclude the possibility that both set of observables can be sensitive to the same physical mechanisms. In the recent theoretical study [?] it was pointed out that the mechanism giving rise to symmetry plane correlations (nonlinear coupling) can also contribute to symmetric cumulants. As a concrete example it was discussed that the existing correlation due to hydrodynamic evolution between V_4 and V_2^2 (which are vectors in the transverse plane) implies that both the angles and the magnitudes are correlated [?].

Interpretation of flow results obtained with multiparticle correlation techniques in small colliding systems, like pp and p-Pb at LHC, remains a challenge. The underlying difficulty stems from the fact that when anisotropic flow harmonic v_n is estimated with k -particle correlator, the statistical spread of that estimate scales to leading order as $\sigma_{v_n} \sim \frac{1}{\sqrt{N}} \frac{1}{M^{k/2}} \frac{1}{v_n^{k-1}}$, where M is the number of particles in an event (multiplicity) and N is total number of events. This generic scaling ensures that multiparticle correlations are precision method only in heavy-ion collisions, characterized both with large values of multiplicity and flow. To leading order the measurements in small systems [? ? ? ? ?] and the measurements in heavy-ion collisions resemble the same features, which can be attributed to collective anisotropic flow in both cases. However, such interpretation is challenged by the outcome of recent Monte Carlo study [?] for e^+e^- systems in which collective effects are not expected. Nonetheless, in this study to leading order multiparticle correlations exhibit yet again the similar universal trends first seen in heavy-ion collisions, both for elliptic and triangular flow. Therefore, it seems unlikely that the analysis of individual flow harmonics with multiparticle techniques will answer whether collective effects can develop and QGP be formed in small systems—instead new observables, like SC, might provide the final answer due to their better sensitivity [? ?].

2.2 Event and Track Selection

The data sample recorded by ALICE during the 2010 heavy-ion run at the LHC is used for this analysis. Detailed descriptions of the ALICE detector can be found in [? ? ?]. The Time Projection Chamber (TPC) was used to reconstruct charged particle tracks and measure their momenta with full azimuthal coverage in the pseudorapidity range $|\eta| < 0.8$. Two scintillator arrays (V0) which cover the pseudo-rapidity ranges $-3.7 < \eta < -1.7$ and $2.8 < \eta < 5.1$ were used for triggering and the determination of centrality [?]. The trigger conditions and the event selection criteria are identical to those described in [? ?]. Approximately 10^7 minimum-bias Pb-Pb events with a reconstructed primary vertex within ± 10 cm from the nominal interaction point in the beam direction are used for this analysis. Charged particles reconstructed in the TPC in $|\eta| < 0.8$ and $0.2 < p_T < 5$ GeV/c were selected. The charged track quality cuts described in [?] were applied to minimize contamination from secondary charged particles and fake tracks. The reconstruction efficiency and contamination of charged particles were estimated from HIJING Monte Carlo simulations [?] combined with a GEANT3 [?] detector model and were found to be independent of the collision centrality. The reconstruction efficiency increases from 70% to 80% for particles with $0.2 < p_T < 1$ GeV/c and remains constant at $(80 \pm 5)\%$ for $p_T > 1$ GeV/c. The estimated contamination by secondary charged particles from weak decays and photon conversions is less than 6% at $p_T = 0.2$ GeV/c and falls below 1% for $p_T > 1$ GeV/c. With this choice of low p_T cut-off we are reducing event-by-event biases from smaller reconstruction efficiency at lower p_T , while the high p_T cut-off of 5 GeV/c was

introduced to reduce the contribution to the anisotropies from jets. Reconstructed tracks were required to have at least 70 TPC space points (out of a maximum of 159). Only tracks with a transverse distance of closest approach (DCA) to the primary vertex less than 3 mm, both in longitudinal and transverse direction, are accepted to reduce the contamination from secondary tracks (for instance the charged particles produced in the detector material, particles from weak decays, etc.). Tracks with kinks (the tracks that appear to change direction due to multiple scattering, K^\pm decays) were rejected.

2.3 Systematic Uncertainties

The systematic uncertainties are estimated by varying the event and track selection criteria. All systematic checks described here are performed independently. All results of $SC(m, n)$ with a selected criterion are compared to ones from the default event and track selection described in the previous section. The differences between the default results and the ones obtained from the variation of the selection criteria are taken as systematic uncertainty of each individual source. The contributions from different sources were then added in quadrature to obtain the final value of the systematic uncertainty.

The event centrality was determined by the V0 detectors [?] with better than 2% resolution of centrality determination. The systematic uncertainty from centrality determination was evaluated by using TPC and Silicon Pixel Detector (SPD) [?] detectors instead of the default, V0 detectors. The systematic uncertainties from the centrality determinations were about 3% both for $SC(5,2)$ and $SC(4,3)$, and 8% for $SC(5,3)$.

As described in Sec. ??, the reconstructed vertex position in beam axis (z -vertex) is required to be located within 10 cm of interaction point (IP) to ensure an uniform detector acceptance for the tracks within $|\eta| < 0.8$ for all the vertices. The systematic uncertainty from z -vertex cut was estimated by reducing the z -vertex to 8cm and was found to be less than 3%.

The analyzed events were recorded with two settings of the magnetic field polarities and the resulting data sets have almost the same number of events. Events with both magnetic polarizations were used for the default analysis and the systematic uncertainties were evaluated from the results from each of two polarized magnetic field settings. Moreover, because of incompleteness of track reconstruction, correction steps are necessary to trace back from reconstructed tracks to the originally generated particles from the collisions. The effects from p_T dependence reconstruction efficiency were taken into systematic uncertainty. Magnetic polarizations and reconstruction efficiency effects are relatively small and difference from the default settings were less than 2%.

The systematic uncertainty due to the track reconstruction was estimated using two additional tracking criteria, first relying on the so-called standalone TPC tracking with the same parameters as described in Sec. ??, and the second that relies on the combination of the TPC and the Inner Tracking System (ITS) detectors with tighter selection criteria. To correct for non-uniform azimuthal acceptance due to dead zones in SPD, and to get the best transverse momentum resolution, approach of hybrid selection with SPD hit and/or ITS refit tracks combined with TPC were used. Then each track reconstruction was evaluated by varying the threshold on parameters used to select the tracks at the reconstruction level. The systematic difference of up to 12% was observed in $SC(m, n)$ results from the different track selections. In addition, we applied the like-sign technique to estimate non-flow effects on $SC(m, n)$. The difference between both charged combinations and like-sign combinations were the largest contribution to the systematic uncertainty and they were about 7% for $SC(4,3)$ and 20% for $SC(5,3)$.

One of the other largest contributions to the systematic uncertainty originates from the non-uniform reconstruction efficiency. In order to estimate the effects on the measurements of these azimuthal correlators for various detector inefficiencies, we use the AMPT models (see the details in Sec. ??) which have flat uniform distribution of azimuthal angles. Then we enforce detector inefficiencies by imposing non-uniform azimuthal distribution from the data. For the observables, $SC(5,2)$, $SC(5,3)$ and $SC(4,3)$,

the uncertainties from the non-uniform distribution of azimuthal angles were about 9%, 17% and 11%, respectively. Generally, systematic uncertainties are larger for the SC(5,3) and SC(5,2) than for the lower harmonics of SC(m,n), because smaller values of v_n are more sensitive to azimuthal modulation and v_n decreases with n increasing.

3 Theoretical models

We have used various models in this article. The HIJING model [?] was utilized to obtain the p_T -weights [?] which were used to estimate systematic bias due to non-uniform reconstruction efficiency. ~~Secondly, the HIJING model was used to estimate the strength of non-flow correlations (typically few-particle correlations insensitive to the collision geometry).~~

We have compared the centrality dependence of our observables with theoretical model from [?], where the initial energy density profiles are calculated using a next-to-leading order perturbative-QCD+saturation model [?]. The subsequent spacetime evolution is described by relativistic dissipative fluid dynamics with different parametrizations for the temperature dependence of the shear viscosity to entropy density ratio $\eta/s(T)$. Each of the $\eta/s(T)$ parametrizations is adjusted to reproduce the measured v_n from central to mid-peripheral collisions.

The VISH2+1 [?] is an event-by-event theoretical framework model for relativistic heavy-ion collision based on (2+1)-dimensional viscous hydrodynamics which describes both the QGP fluid and the highly dissipative and even off-equilibrium late hadronic stage with fluid-dynamics. With well tuned transport coefficients, decoupling temperature and some well-chosen initial conditions (like AMPT [?] etc.), it could fit many related soft hadron data, such as the p_T spectra and different flow harmonics at RHIC and the LHC [?]. Three different initial conditions (MC-Glauber, MC-KLN and AMPT) along with different constant η/s parametrizations are used in the model [?]. Traditionally, the Glauber model constructs the initial entropy density of the QGP fireball from a mixture of the wounded nucleon and binary collision density profiles [?], and the KLN model assumes the initial entropy density is proportional to the initial gluon density calculated from the corresponding k_T factorization formula [?]. In the Monte-Carlo versions (MC-Glauber and MC-KLN) [?], additional initial state fluctuations are introduced through the position fluctuations of individual nucleons inside the colliding nuclei. For the AMPT initial conditions [?], the fluctuating energy density profiles are constructed from the energy decompositions of individual partons, which fluctuate in both momentum and position space. Compared with the MC-Glauber and MC-KLN initial conditions, the additional Gaussian smearing parameter in the AMPT initial conditions makes the typical initial fluctuation scales changeable which gives rise to non-vanishing initial local flow velocities [?].

Finally, we provide an independent estimate of the centrality dependence of our observables by utilizing the AMPT model [?]. Even though thermalization could be achieved in collisions of very large nuclei and/or at extremely high energy, the dense matter created in heavy-ion heavy-ion collisions may not reach full thermal or chemical equilibrium as a result of its finite volume and energy. To address such non-equilibrium many-body dynamics, AMPT has been developed, which includes both initial partonic and final hadronic interactions and the transition between these two phases of matter. For the initial conditions, the AMPT model uses the spatial and momentum distributions of hard minijet partons and soft strings from the HIJING model [?]. The AMPT model can be run in two main configurations, the default and the string melting model. In the default version, partons are recombined with their parent strings when they stop interacting. The resulting strings are later converted into hadrons using the Lund string fragmentation model [?]. In the string melting version, the initial strings are melted into partons whose interactions are described by the ZPC parton cascade model [?]. These partons are then combined into the final-state hadrons via a quark coalescence model. In both configurations, the dynamics of the subsequent hadronic matter is described by a hadronic cascade based on a Relativistic

Transport (ART) model [?] which also includes resonance decays. The third version presented in this article is based on the string melting configuration, in which the hadronic rescattering phase is switched off to study its influence to the development of anisotropic flow. The input parameters used in both configurations are: $\alpha_s = 0.33$, a partonic cross-section of 1.5 mb, while the Lund string fragmentation parameters were set to $\alpha = 0.5$ and $b = 0.9 \text{ GeV}^{-2}$. Even though the string melting version of AMPT [?] reasonably reproduces particle yields, p_T spectra, and v_2 of low- p_T pions and kaons in central and mid-central Au–Au collisions at $\sqrt{s_{NN}} = 200 \text{ GeV}$ and Pb–Pb collisions at $\sqrt{s_{NN}} = 2760 \text{ GeV}$ [?], it was seen clearly in the recent study [?] that it fails to quantitatively reproduce the measurements. It turns out that the radial flow in AMPT is 25% lower than the measured value at the LHC, which indicates that the unrealistically low radial flow in AMPT is responsible for the quantitative disagreement. The detail configurations on AMPT settings used for this article and the comparisons of p_T differential v_n for pions, kaons and protons to the data can be found in [?].

4 Results

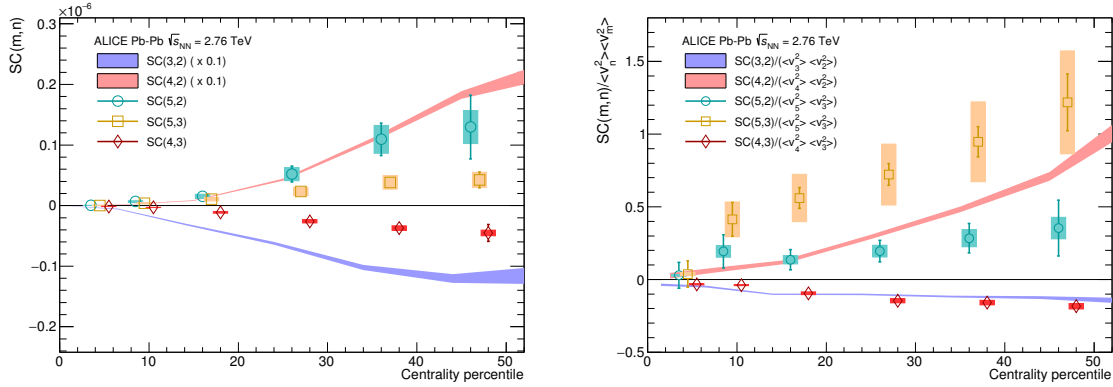


Fig. 1: The result of $SC(m,n)$ (left figure) and $NSC(m,n)$ (right figure) with flow harmonic order up to 5th in Pb–Pb $\sqrt{s_{NN}} = 2.76 \text{ TeV}$. Note that the lower order harmonic correlations ($SC(4,2), SC(3,2)$) are scaled down by factor of 10 and only statistical errors are shown in the left hand side figure.

The centrality dependence of $SC(4,2)$ and $SC(3,2)$ are presented in Fig. ?? as shadow bands which are the same as the published results [?]. Positive values of $SC(4,2)$ are observed for all measured centralities. This suggests a positive correlation between the event-by-event fluctuations of v_2 and v_4 . It also indicates that finding v_2 larger than average ($\langle v_2 \rangle$) in an event enhances the probability of finding v_4 larger than average ($\langle v_4 \rangle$) in that event. On the other hand, the negative results of $SC(3,2)$ over all measured centralities show the anti-correlation between v_2 and v_3 flow harmonic magnitudes, which further implies that finding v_2 larger than average ($v_2 > \langle v_2 \rangle$) enhancing the probability of finding smaller v_3 than average ($v_3 < \langle v_3 \rangle$).

The centrality dependence of the higher order harmonic correlations ($SC(4,3)$, $SC(5,2)$ and $SC(5,3)$) are presented in Fig. ?? and compared to the lower order harmonic correlations ($SC(4,2), SC(3,2)$) which are the same as the published results [?]. The correlation between v_3 and v_4 is negative as similarly as v_3 and v_2 while the others are all positive, which reveals that v_2 and v_5 , v_3 and v_5 are correlated as v_2 and v_4 , while v_3 and v_4 are anti-correlated as v_3 and v_2 . The higher order flow harmonic correlations ($SC(4,3)$, $SC(5,2)$ and $SC(5,3)$) are much smaller compared to the lower order harmonics ($SC(3,2)$ and $SC(4,2)$). Especially $SC(5,2)$ is 10 times smaller than $SC(4,2)$ and $SC(4,3)$ is about 20 times smaller than $SC(3,2)$.

However, unlike $SC(m,n)$, $NSC(m,n)$ results with the higher order flow harmonics show almost same order of the correlation strength as the lower order flow harmonic correlations ($NSC(3,2)$ or $NSC(4,2)$).

NSC(4,3)) is comparable to NSC(3,2) and one finds that a hierarchy $\text{NSC}(5,3) > \text{NSC}(4,2) > \text{NSC}(5,2)$ holds for most of centrality ranges within the errors. These results indicate that the lower order harmonic correlations (SC(3,2) and SC(4,2)) are larger than higher order harmonic correlations (SC(4,3), SC(5,2) and SC(5,3)), not only because of the correlation strength itself but also the individual flow strength. SC(5,2) is stronger than SC(5,3), but as for NSC, the correlation between v_5 and v_3 is stronger than the correlation between v_5 and v_2 .

To obtain the p_T dependence of SC(m,n) results, we apply minimum p_T cuts, instead of p_T bin-by-bin interval in order to avoid large statistical fluctuations in the results. The various minimum p_T cuts from 0.2 to 1.5 are applied. The results of p_T dependence with SC(3,2) and SC(4,2) for minimum p_T cuts, $0.2 < p_T < 0.7$, are shown on the left top in Fig. ???. The strength of SC(m,n) correlation becomes larger as the minimum p_T increases. This indicates that the relationship between event-by-event fluctuation of two different flow harmonics v_m and v_n is stronger for high p_T particles. This p_T dependence correlations have much stronger centrality dependence, where SC(m,n) gets much larger as the centrality or p_T increase. NSC(3,2) and NSC(4,2) with different minimum cuts are shown on the right in Fig. ???. The strong p_T dependence observed in SC(m,n) is not clearly seen in NSC(m,n). NSC(m,n) results are aligned all together and consistent in errors for all minimum p_T cuts. This suggests that the p_T dependence of SC(m,n) does not solely result from the correlation between flow harmonics but results from the different values of p_T dependent individual v_n values. The minimum p_T cuts are extended from 0.8 to 1.5 GeV/ c and the results are shown on the bottom in Fig. ???. As for SC(m,n), the similar trends are observed as similarly as $p_T < 0.8$, however NSC(m,n) tends to decrease as the minimum p_T or the centrality increase. The p_T dependence for NSC(3,2) is not clearly seen and it is consistent with no p_T dependence within the current statistical and systematic errors except for 40-50% centrality and NSC(4,2) shows a moderate decreasing trend for increasing p_T (see further discussions in Sec. ??). This might be an indication of possible viscous corrections for the equilibrium distribution at hadronic freeze-out [?].

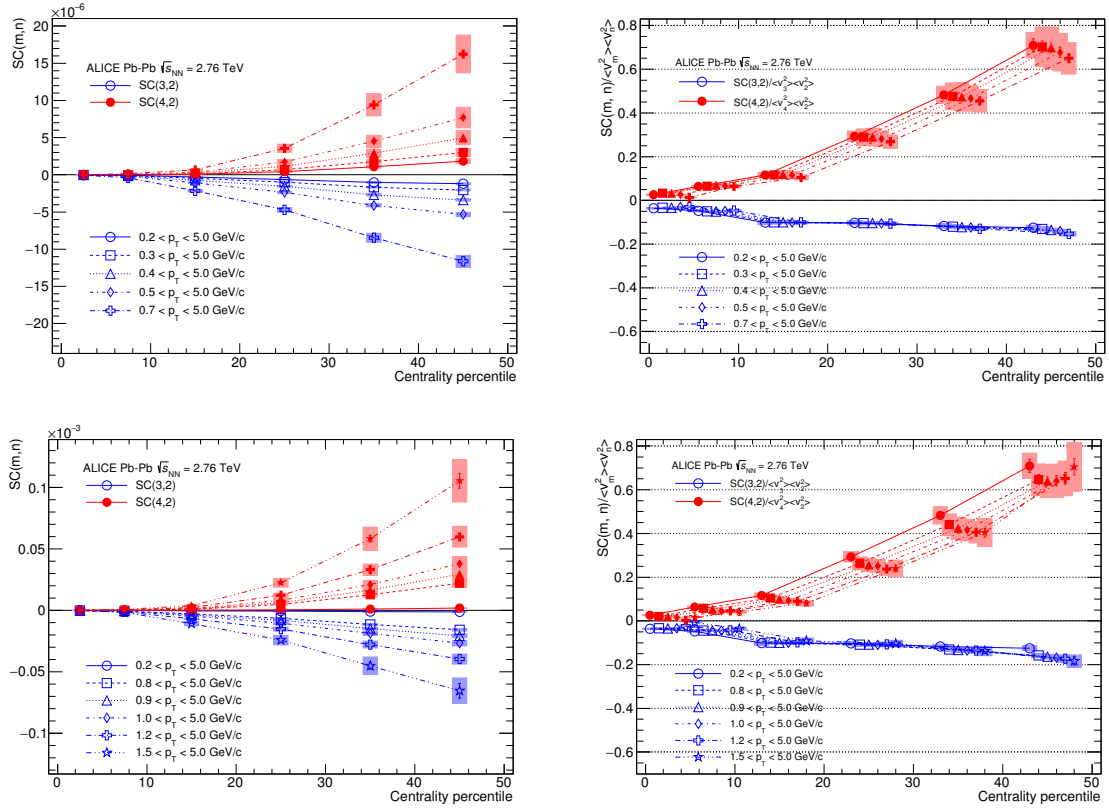


Fig. 2: $SC(3,2)$ and $SC(4,2)$ with various minimum p_T cuts (left) and results of normalized $SC(3,2)$ and $SC(4,2)$ (right). The upper panels show the results for minimum p_T range, $0.2 < p_T < 0.7$ GeV/c and the bottom panels are for minimum p_T range, $0.8 < p_T < 1.5$ GeV/c. Note that NSC data points from each minimum p_T in a centrality percentile bin are shifted for visibility.

5 Model ~~comparisons~~Comparisons

5.1 Low ~~order harmonic correlations~~Order Harmonic Correlations

SC(3,2) and SC(4,2) are compared to several theoretical calculations. First, the fluid hydrodynamic predictions with the different parameterizations for the temperature dependence of the shear viscosity to entropy ratio $\eta/s(T)$ are shown on the left in Fig. ?? . ~~The hydrodynamic calculations roughly capture qualitatively the centrality dependence, but not quantitatively. Both SC(3,2) with data and hydrodynamics have negative values for all centralities, while SC(4,2) results have positive values over all measured centralities. However, there is no single centrality for which a given $\eta/s(T)$ parameterization describes both SC(3,2) and SC(4,2) simultaneously. On the other hand, the same hydrodynamic calculations capture the centrality dependence of the individual v_n quantitatively [?].~~

~~NSC(3,2) and NSC(4,2) are also compared to the same model on the right in Fig. ?? . While NSC(3,2) does not show sensitivity to different $\eta/s(T)$ parameterizations, NSC(4,2) exhibit much better sensitivity than NSC(3,2) observable and the individual flow harmonics [?]. These findings indicate in Fig2 in Ref. [?]. It has been demonstrated that NSC(3,2) observable is sensitive mainly to the initial conditions, while NSC(4,2) observable is sensitive to both the initial conditions and the system properties, which is consistent with the prediction from [?]. However, the sign of NSC(3,2) is positive in the models in 0-10% central collisions while it is negative in data. In the most central collisions the anisotropies originate mainly from fluctuations, i.e. the initial ellipsoidal geometry characteristic for mid-central collisions plays little role in this regime. Hence this observation will help to understand the fluctuations in initial conditions better. NSC(4,2) observable shows better sensitivity for different $\eta/s(T)$ parameterizations, i.e. medium property but the model cannot describe the centrality dependence nor the absolute values. These observed distinct discrepancies between data and models might indicate that the current understanding of initial conditions used in the model need to be revisited to further constrain the $\eta/s(T)$, considering the difficulties on separating the role of the η/s from the initial condition to the final state particle anisotropies [? ?]. Hence the use of SC(m,n) and NSC(m,n) can provide new constraints on the detailed modeling of the initial-state condition and the fluctuations of the medium created in heavy ion-heavy-ion collisions and the better constraints on the initial-state conditions will certainly improve the uncertainties of determining $\eta/s(T)$.~~

~~Results from SC(m,n) in Pb-Pb $\sqrt{s_{NN}} = 2.76$ TeV are compared to hydrodynamic calculations. The dashed lines are hydrodynamic predictions with various $\eta/s(T)$ parametrizations [?].~~

The results with the comparison to VISH2+1 calculation are shown in Fig. ?? . All the models with the large share viscosity regardless of the initial conditions ($\eta/s = 0.2$ for MC-KLN and MC-Glauber initial conditions and $\eta/s = 0.16$ for AMPT initial condition) fails to capture the centrality dependence of SC(3,2) and SC(4,2). And among the models with small shear viscosities ($\eta/s = 0.08$), the one with the AMPT initial condition describes the data better both for SC(3,2) and SC(4,2) but they cannot describe the data quantitatively for most of the centrality ranges. As similarly as the above mentioned hydrodynamic calculations [?], the sign of the normalised NSC(3,2) in these models is opposite to the data in 0-10% central collisions. NSC(3,2) does not show sensitivity to initial conditions or η/s parametrizations and cannot be described by these models quantitatively. However, for NSC(4,2), it is sensitive both to initial conditions and η/s parametrizations. Even though NSC(4,2) is favoured both by AMPT initial condition with $\eta/s=0.08$ and MC-Glauber initial condition with $\eta/s = 0.20$, SC(4,2) can be only described by smaller η/s from AMPT and MC-Glauber initial conditions. Therefore the Glauber initial condition with $\eta/s = 0.20$ model can be ruled out and we come to a conclusion based on the tested model parameters that η/s should be small and AMPT initial condition is favoured by the data.

Finally, the extracted results from particle level AMPT simulations in the same way as for the data are compared to the data in Fig. ?? . As for SC(3,2), neither of the settings can describe the data and the

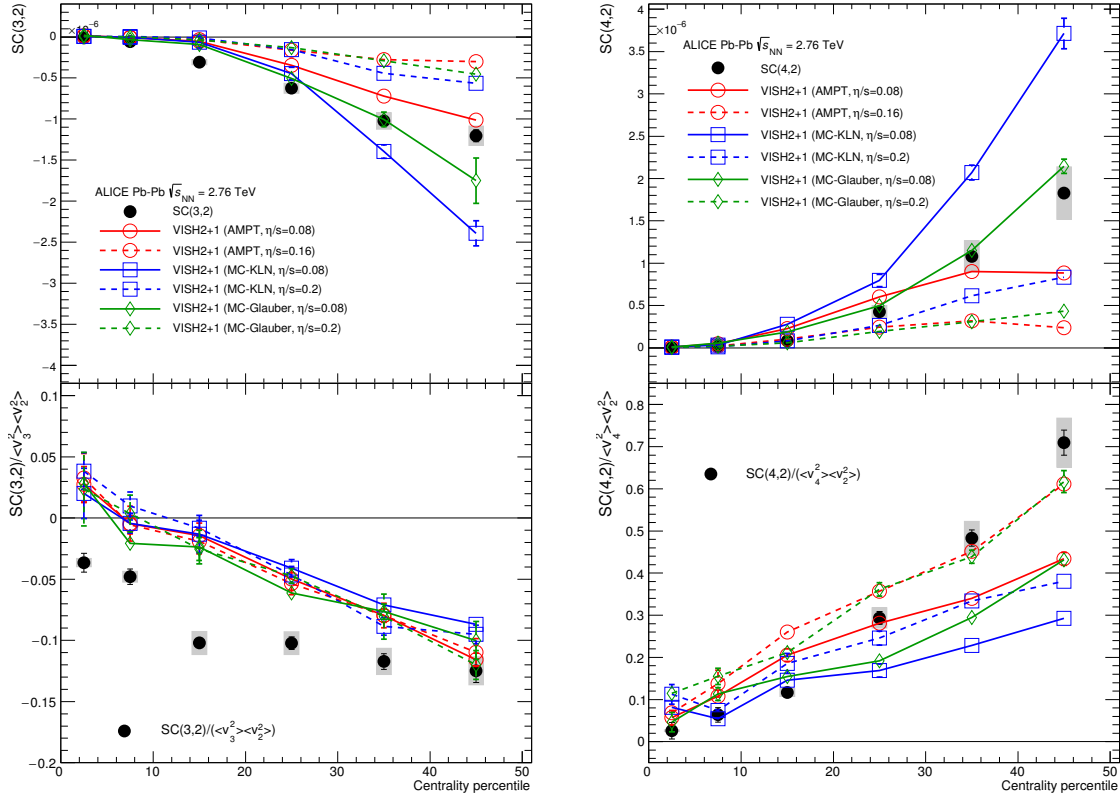


Fig. 3: Results of $SC(3,2)$ and $SC(4,2)$ are compared to various VISH2+1 calculations [?] with different settings. Three initial conditions from AMPT, MC-KLN, and MC-Glauber are drawn as different colors and markers. The η/s parameters are shown as different line styles, the small shear viscosities ($\eta/s = 0.08$) are shown as solid lines, and large shear viscosities ($\eta/s = 0.2$ for MC-KLN and MC-Glauber, 0.16 for AMPT) are drawn as dashed lines. Upper panels are the result of $SC(m,n)$ and lower panels are the results of $NSC(m,n)$.

setting with the default AMPT model somewhat follows the trend of the data closest. The same setting
 385 can describe NSC(3,2) fairly well and also the sign of NSC(3,2) is well reproduced by this setting while
 all the hydrodynamic calculations in this article failed to describe the sign of the observable in the most
 central collisions. Interestingly the string melting AMPT model cannot capture the data well where
 the strength of the correlation is weaker than the default model. The third version based on the string
 melting configuration with the hadronic rescattering phase off is also shown to quantify its influence.
 390 This late hadronic rescattering stage makes both SC(3,2) and NSC(3,2) stronger in the string melting
 AMPT model but it is not enough to describe the data. Further we investigated why the default AMPT
 model can describe NSC(3,2) fairly well but underestimates SC(3,2). By taking the differences in the
 individual flow harmonics (v_2 and v_3) between the model and data into account, we were able to recover
 the difference in SC(3,2) between the data and the model. The discrepancy in SC(3,2) can be explained
 395 by the overestimated individual v_n values reported in [?] in all the centrality ranges.

In the case of SC(4,2), the string melting AMPT model can fairly well describe the data while the de-
 fault model underestimates it. NSC(4,2) is slightly overestimated by the same setting which can describe
 SC(4,2) but the default AMPT model can describe the data better. The influence of the hadronic rescat-
 tering phase for NSC(4,2) is opposite to other observables (SC(3,2), NSC(3,2) and SC(4,2)), where
 400 the hadronic rescattering make NSC(4,2) slightly smaller. It should be noted that the better agreement
 for SC(m,n) should not be overemphasized since there are discrepancies in the individual v_n between
 AMPT and data as it was demonstrated for SC(3,2). Hence the simultaneous description of SC(m,n) and
 NSC(m,n) should give better constraints to the parameters in AMPT.

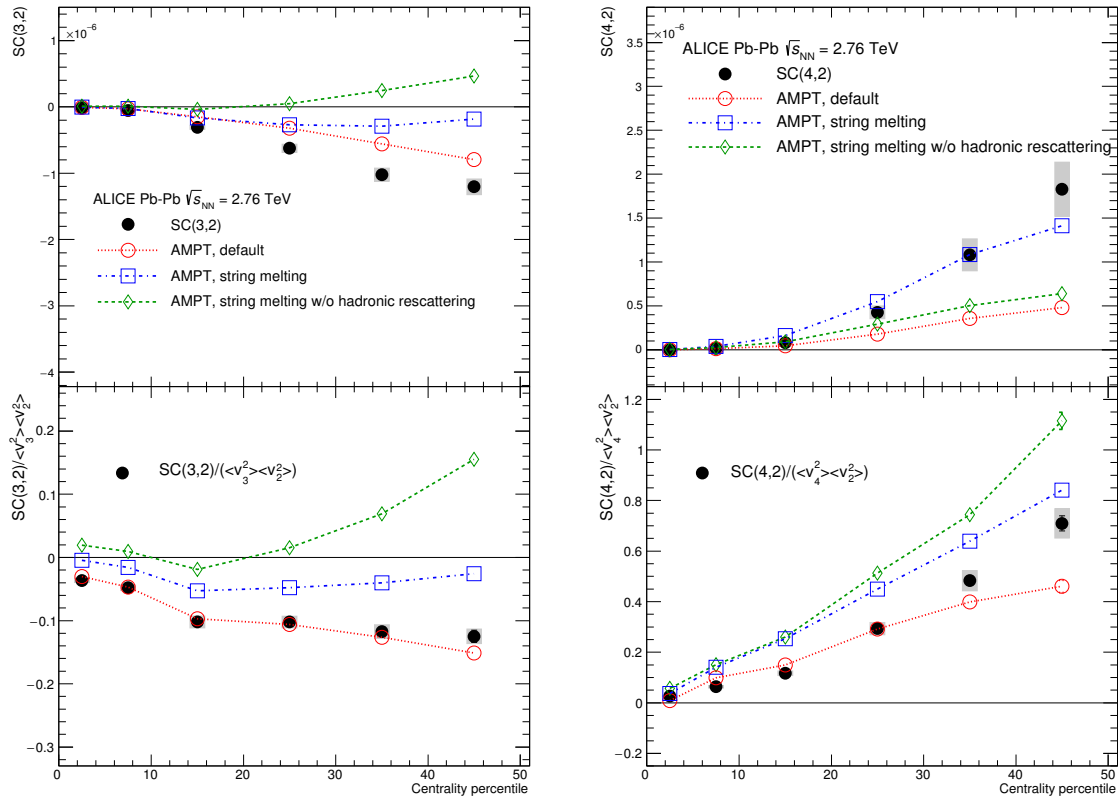


Fig. 4: Results of $SC(3,2)$ and $SC(4,2)$ are compared to various AMPT simulations. Upper panels are the results of $SC(m,n)$ and the lower panels are the results of $NSC(m,n)$. The details of the AMPT configurations can be found in Sec. ??.

5.2 Higher order harmonic correlations

The higher order harmonic correlations (SC(4,3), SC(5,2) and SC(5,3)) are compared to several theoretical calculations. First, the fluid hydrodynamic predictions with the different parameterizations for the temperature dependence of the shear viscosity to entropy ratio $\eta/s(T)$ are shown on the left in Fig. ??.

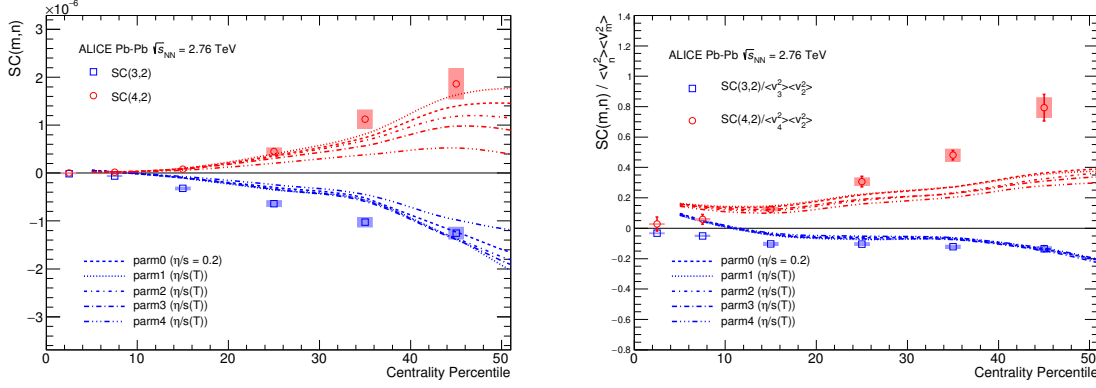


Fig. 5: Results from SC(m,n) in Pb-Pb $\sqrt{s_{NN}} = 2.76$ TeV are compared to hydrodynamic calculations. The dashed lines are hydrodynamic predictions with various $\eta/s(T)$ parametrizations [?]. This will be replaced with new figures once we have the calculations for Harri

The higher order harmonic correlations (SC(4,3), SC(5,2) and SC(5,3)) are compared to VISH2+1 calculation calculations [?], shown in Fig. ??.

All the models with the large share viscosity regardless of the initial conditions ($\eta/s = 0.2$ for MC-KLN and MC-Glauber initial conditions, and $\eta/s = 0.16$ for AMPT) failed to capture the centrality dependence of SC(5,2), SC(5,2) and SC(5,3), more clearly than lower order harmonic correlations (SC(3,2), SC(4,2)). And among the models with small shear viscosity ($\eta/s = 0.08$), the one from the AMPT initial condition describes the data much better than the other initial conditions. A quite clear separation between different initial conditions is observed for these higher order harmonics harmonic correlations compared to the lower order harmonic correlations. NSC(5,2) and SC(5,3) are quite sensitive to both the initial conditions and the η/s parametrizations. As similarly as the above mentioned hydrodynamic calculations [?], the sign of the normalised NSC(4,3) in these models is opposite to the data in 0-10% central collisions. NSC(4,3) shows sensitivity to both initial conditions and η/s parametrizations while NSC(3,2) didn't show sensitivity to initial conditions or η/s parametrizations. SC(4,3) data is clearly favoured by smaller η/s but NSC(4,3) cannot be described by these models quantitatively.

The extracted results from particle level AMPT simulations in the same way as for the data are compared to the data in Fig. ??.

The string melting AMPT model describes SC(5,2) and SC(5,3) well. The same setting describes only NSC(5,3) but it overestimates NSC(5,2). However the default AMPT model can describe NSC(5,3) and NSC(5,2) fairly well as similarly as NSC(3,2) and NSC(4,2).

In the case of SC(4,3), neither of the settings can describe the data but the default AMPT model follows the data closest. The string melting AMPT model fails to describe SC(4,3) and NSC(4,3). In summary, the default AMPT model describes the normalized SC (NSC(m,n)) from lower to higher order harmonic correlation while the string melting AMPT model overestimates NSC(5,2) and underestimates (or very weak correlations) NSC(4,3).

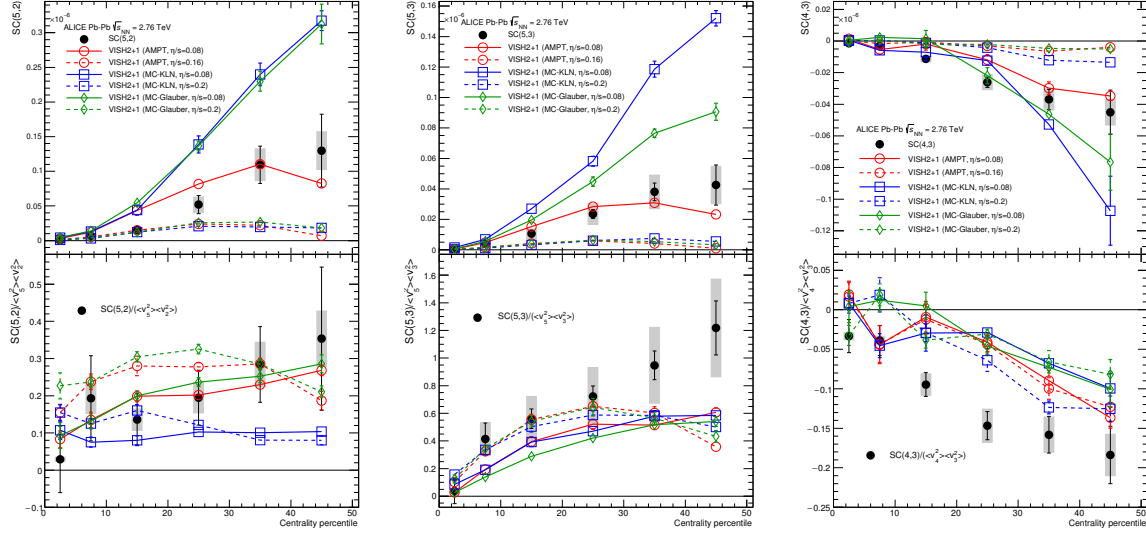


Fig. 6: Results of $SC(5,2)$, $SC(5,3)$ and $SC(4,3)$ are compared to various VISH2+1 calculations [?]. Three initial conditions from AMPT, MC-KLN and MC-Glauber are drawn as different colors and markers. The η/s parameters are shown as different line styles, the small shear viscosity ($\eta/s = 0.08$) are shown as solid lines, and large shear viscosities ($\eta/s = 0.2$ for MC-KLN and MC-Glauber, 0.16 for AMPT) are drawn as dashed lines. Upper panels are the results of $SC(m,n)$ and lower panels are the results of $NSC(m,n)$.

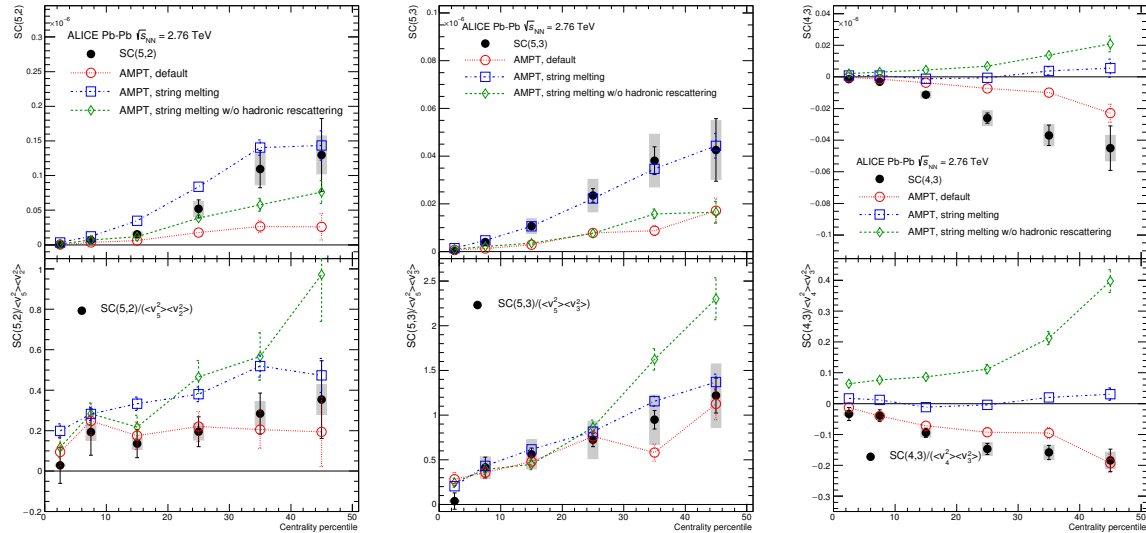


Fig. 7: Results of $SC(5,2)$, $SC(5,3)$ and $SC(4,3)$ are compared to various AMPT simulations. Upper panels are the results of $SC(m,n)$ and the lower panels are the results of $NSC(m,n)$. The details of the AMPT configurations can be found in Sec. ??.

5.3 **Transverse momentum dependence** Momentum Dependence of Low **order-harmonic correlations** Order Harmonic Correlations

NSC(3,2) and NSC(4,2) as a function of different minimum p_T cut are compared to the AMPT simulations in Fig. ???. As discussed in Sec. ??, the p_T dependence for NSC(3,2) and NSC(4,2) in mid central collisions is seen also in AMPT simulations for higher minimum p_T cuts. The other AMPT configurations except for the default AMPT model give very strong p_T dependence above 1 GeV/ c and cannot describe the magnitude of the data both for NSC(3,2) and NSC(4,2). In the case of NSC(3,2), the default AMPT model describes the magnitude and p_T dependence well in all collision centralities except for 40 – 50% where the model underestimates the data and have stronger p_T dependence than the data. As for NSC(4,2), the same model which describes NSC(3,2) also can reproduce the data well expect for 10 – 20% and 40 – 50% centralities where some deviations from the data both for the magnitude and p_T dependence are observed. When the string melting AMPT model is compared to the same model with the hadronic rescattering off, it is observed that the very strong p_T dependence as well as the correlation strength get weaker by the hadronic rescattering. This might imply that the hadronic interaction is the source of this observed p_T dependence even though the relative contributions from partonic and hadronic stage in the final state particle should be studied further. This observed moderate p_T dependence in mid central collisions both for NSC(3,2) and NSC(4,2) might be an indication of possible viscous corrections for the equilibrium distribution at hadronic freeze-out predicted in [?].

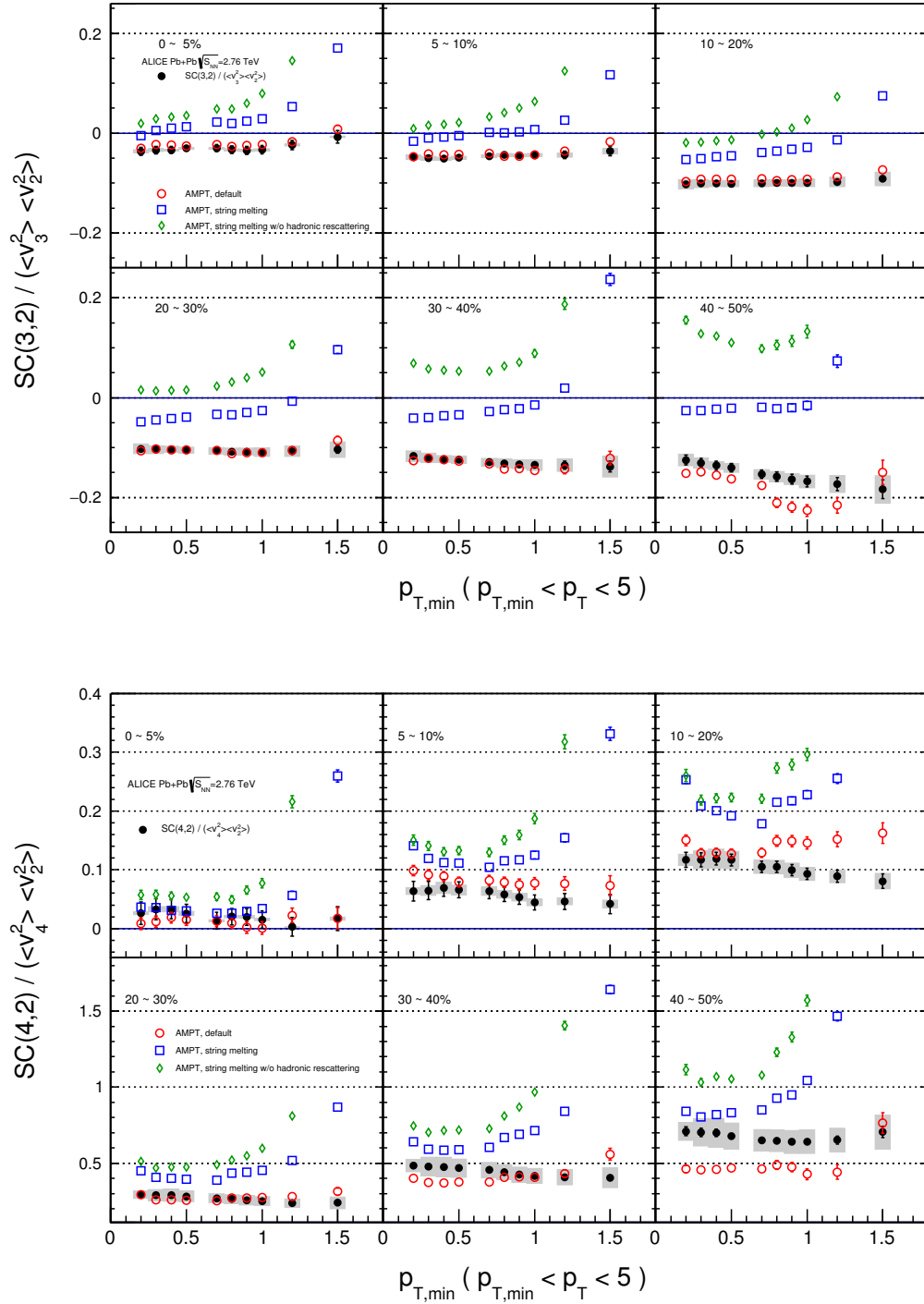


Fig. 8: NSC(3,2) (Top) and SC(4,2) (Bottom) as a function of minimum p_T cuts. The AMPT results are drawn as color bands for comparison. The details of the AMPT configurations can be found in Sec. ??.

6 Summary

In summary, we have measured the Symmetric 2-harmonic 4-particle Cumulants (SC), which quantify the relationship between event-by-event fluctuations of two different flow harmonics. The observables are particularly robust against few-particle non-flow correlations and they provide orthogonal information to recently analysed symmetry plane correlators. We have found that fluctuations of v_2 and v_3 (v_3 and v_4) are anti-correlated in all centralities and fluctuations of v_2 and v_4 (v_2 and v_5 , v_3 and v_5) are correlated for all centralities. This feature was explored to discriminate between various hydro model calculations with different initial conditions as well as different parametrizations of the temperature dependence of η/s . We have found that the different order harmonic correlations have different sensitivities to the initial conditions and the system properties. Therefore they have discriminating power on separating the role of the η/s from the initial condition to the final state particle anisotropies. Furthermore, the sign of v_3 - v_2 correlation in the model in 0-10% central collisions was found to be different between the data and hydrodynamic model calculations. In the most central collisions the anisotropies originate mainly from fluctuations, i.e. the initial ellipsoidal geometry characteristic for mid-central collisions plays little role in this regime. Hence this observation might help to understand the details of the fluctuations in initial conditions. The comparisons to VISH2+1 calculation show that all the models with the large share viscosity regardless of the initial conditions failed to capture the centrality dependence of higher order correlations, more clearly than lower order harmonic correlations and based on the tested model parameters that the η/s should be small and AMPT initial condition is flavored by the data. A quite clear separation of the correlation strength between different initial conditions is observed for these higher order harmonic correlations compared to the lower order harmonic correlations. Finally we have found that v_3 - v_2 and v_4 - v_2 correlations have moderate p_T dependence in mid central collisions. This might be an indication of possible viscous corrections for the equilibrium distribution at hadronic freeze-out. The results presented in this article can be used to further optimize model parameters and put better constraints on the initial conditions and the transport properties in ultra-relativistic heavy-ion collisions.

Acknowledgements

A The ALICE Collaboration